Location, Size and Orientation Effect of Semi-elliptical Surface Crack on the Fracture of a Type-3 Composite Pressure Vessel using *J*-integral Method

Muzaffer Çetin[#] and Kemal Yaman[*]

[#]*Space Technologies Research Institute,*
The Scientific and Technological Research Council of Turkey, Ankara - 06800, Turkey
[*]*Defense Industries Research and Development Institute,*
The Scientific and Technological Research Council of Turkey, Ankara - 06261, Turkey
[*]*E-mail: kemal.yaman@tubitak.gov.tr*

ABSTRACT

In this study, structural design and analysis of a type-3 composite over wrapped pressure vessel used in a military satellite propulsion system is presented. The aim is to design a composite tank lighter than all metal fuel tanks having the same volume. Moreover, necessary design stages have been revealed for similar composite over wrapped pressure vessels. ANSYS® is used to perform the stress-strain analysis of both metal and composite parts, to determine the optimum winding angle, tank Autofrettage and fracture characteristic for the metal liner considering the crack morphology. Tsai-Hill, Tsai-Wu and Hashin theories have been implemented to investigate the various failure modes of the composite vessel. Location, size and orientation angle of semi-elliptical surface crack has a pronounced effect on fracture characteristic of the liner. In fracture investigation *J*-integral method is used. It is foreseen that even in the most critical crack, the crack will not propagate and there will be no burst in the tank for proposed loading conditions. Numerical results are good agreement with the experimental results.

Keywords: Autofrettage; Crack propagation; Failure modes; Filament wound; Fracture mechanics; Pressure vessel

1. INTRODUCTION

A wide range of composite materials are developed to meet the requirements of lightness and high durability. Besides, significant improvements in composite production technologies and reductions in costs have increased the preferability of such materials[1].

To decrease the launching costs, composite materials are utilised in many structural elements on the missiles, satellites, and aerospace vehicles. These structural elements may be load carrying elements (primary structures) but may also be light-weight parts as well. Previously, fuel tanks manufactured from metallic materials used in the space vehicles have a significant weight. Nowadays, they are produced by using lighter composites having 40-50% of their weight. Generally, these tanks are known as "Type 3" and have a thin metal inner liner. While the metal liner ensures that the fuel stored in the tank is sealed, the composite section increases the resistance of the tank to high pressure and environmental loads. The most preferred manufacturing process of this type of tank is called as filament winding. With this method, the winding process is carried out by determining the filament winding angles on an axial symmetrical part to meet the desired strength requirements. For this reason, the design and production stages of composite winding pressure tanks are more complicated process than the tanks which are completely metal[2].

In many engineering applications, crack propagation, which is the result of fatigue, is a very important factor in design processes. Kaikai[3], *et al*. studied the semi-elliptic surface crack model theoretically and applied on the 7075-T6 aluminum plate experimentally. Five different early stage cracks were examined. They were stated that the initial crack aspect ratio, crack depth and half crack length control the surface crack propagation. Xu[4], *et al*. studied wrapped 6061-T6 Carbon-fiber/Epoxy resin oval-shaped pressure vessels with different winding angles. The structure was modelled numerically according to maximum stress, Hoff-man, Tsai-Hill and Tsai-Wu fatigue criteria for analysing the burst pressures. They reported that the Tsai-Wu criteria gave the closest value in above criteria.

The *J*-integral method is used to determine the amount of change in potential energy resulting from the propagation of a crack for elastic-plastic materials. Therefore, it is an indication of whether there will be a propagation in the crack or not. Wang[5], *et al*. investigated the *J*-integral parameter for predicting the crack growth rate for 304 SS material. They show that, the theoretical and experimental crack grow rates are very close to the data obtained by *J*-integral method. In many studies, it is stated that, the *J*-integral or stress intensity factor decreases with increasing the crack height/length ratio[5-8]. Orientation and location of the crack are the other important factors affecting the crack initiation and propagation.

For instance, Fakoor,[9]*et al*. concentrated on the orientation

of the crack. They found that, Longitudinal cracks in pressure vessels are more critical than transverse and another crack orientation. The literature studies[10-13] related to the crack location show that the cylinder dome transition (CDT) regions which have the highest stress and strain values are more critical in terms of crack propagation. To understand the mechanism of crack initiation and propagation, some theoretical background is given.

1.1 Material Model for Composite Structures

1.1.1 Stress-strain relation

To carry out structural analysis of composite wounded tanks, it is necessary to know the stress-strain relation of a composite structure. For this purpose, generalised Hooke law is used. For the strength calculation of a three-dimensional anisotropic body, Hooke's law ($\sigma_i = C_{ij}\varepsilon_j$) is written as follows[1,4,6,13].

$$\begin{bmatrix} \sigma_1 \\ \sigma_2 \\ \sigma_3 \\ \sigma_4 \\ \sigma_5 \\ \sigma_6 \end{bmatrix} = \begin{bmatrix} C_{11} & C_{12} & C_{13} & C_{14} & C_{15} & C_{16} \\ C_{21} & C_{22} & C_{23} & C_{24} & C_{25} & C_{26} \\ C_{31} & C_{32} & C_{33} & C_{34} & C_{35} & C_{36} \\ C_{41} & C_{42} & C_{43} & C_{44} & C_{45} & C_{46} \\ C_{51} & C_{52} & C_{53} & C_{54} & C_{55} & C_{56} \\ C_{61} & C_{62} & C_{63} & C_{64} & C_{65} & C_{66} \end{bmatrix} \begin{bmatrix} \varepsilon_1 \\ \varepsilon_2 \\ \varepsilon_3 \\ \varepsilon_4 \\ \varepsilon_5 \\ \varepsilon_6 \end{bmatrix} \tag{1}$$

The matrix [C] given in Eqn. (1) is expressed as the rigidity (Stiffness) matrix and can be written in the form of the matrix. Hooke's law can be expressed in terms of unit elongation ($\varepsilon_i = S_{ij}\sigma_j$) as the inverse of the matrix [C] of the compliance [S] matrix as given in (2). If there are symmetrical properties in the material according to the three perpendicular planes, these materials are called orthogonal anisotropic materials, i.e., orthotropic material. For an orthotropic material, Hooke's law can be written as shown in Eqn. (2)

$$\begin{bmatrix} \varepsilon_1 \\ \varepsilon_2 \\ \varepsilon_3 \\ \gamma_{23} \\ \gamma_{31} \\ \gamma_{12} \end{bmatrix} = \begin{bmatrix} S_{11} & S_{12} & S_{13} & 0 & 0 & 0 \\ S_{21} & S_{22} & S_{23} & 0 & 0 & 0 \\ S_{31} & S_{32} & S_{33} & 0 & 0 & 0 \\ 0 & 0 & 0 & S_{44} & 0 & 0 \\ 0 & 0 & 0 & 0 & S_{55} & 0 \\ 0 & 0 & 0 & 0 & 0 & S_{66} \end{bmatrix} \begin{bmatrix} \sigma_1 \\ \sigma_2 \\ \sigma_3 \\ \tau_{23} \\ \tau_{31} \\ \tau_{12} \end{bmatrix} \tag{2}$$

The relation given in Eqn. (3) becomes (4) when the engineering constants are written. Here, E, G and v are Modulus of elasticity, Shear modulu and Poisson's ratio respectively.
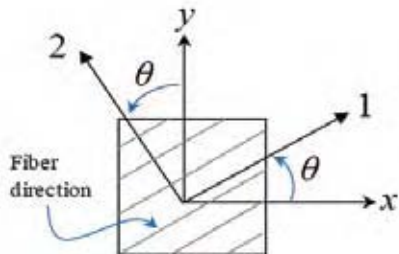

Figure 1. Fiber angle of a composite layer in the planar stress condition and the axis assembly.

$$\begin{bmatrix} \varepsilon_1 \\ \varepsilon_2 \\ \varepsilon_3 \\ \gamma_{23} \\ \gamma_{31} \\ \gamma_{12} \end{bmatrix} = \begin{bmatrix} \dfrac{1}{E_1} & -\dfrac{v_{21}}{E_2} & -\dfrac{v_{31}}{E_3} & 0 & 0 & 0 \\ -\dfrac{v_{12}}{E_1} & \dfrac{1}{E_2} & -\dfrac{v_{32}}{E_3} & 0 & 0 & 0 \\ -\dfrac{v_{13}}{E_1} & -\dfrac{v_{23}}{E_2} & \dfrac{1}{E_3} & 0 & 0 & 0 \\ 0 & 0 & 0 & \dfrac{1}{G_{23}} & 0 & 0 \\ 0 & 0 & 0 & 0 & \dfrac{1}{G_{31}} & 0 \\ 0 & 0 & 0 & 0 & 0 & \dfrac{1}{G_{12}} \end{bmatrix} \begin{bmatrix} \sigma_1 \\ \sigma_2 \\ \sigma_3 \\ \tau_{23} \\ \tau_{31} \\ \tau_{12} \end{bmatrix} \tag{3}$$

Generally, if the ratio of the radius of a cylindrical pressure tank to the wall thickness is greater than 10, this structure is considered to be a thin walled structure. In this case, the plane stress condition is provided and $\sigma_3 = \tau_{13} = \tau_{23} = 0$ for orthotropic material. Thus, the correlations as given in Eqns. (1), (2) and (3) are transformed as[14]:

$$\begin{bmatrix} \varepsilon_1 \\ \varepsilon_1 \\ \gamma_{12} \end{bmatrix} = \begin{bmatrix} \dfrac{1}{E_1} & -\dfrac{v_{21}}{E_2} & 0 \\ -\dfrac{v_{12}}{E_1} & \dfrac{1}{E_2} & 0 \\ 0 & 0 & \dfrac{1}{G_{12}} \end{bmatrix} \begin{bmatrix} \sigma_1 \\ \sigma_2 \\ \tau_{12} \end{bmatrix} \tag{4}$$

Under plane stress condition, the x-y coordinate plane must be transformed into the coordinate system represented by 1-2. As shown in Fig. 1, the axis indicated by 1 is the fibre direction and the axis indicated by 2 is the axis perpendicular to it. To increase the strength of the composite materials in the desired directions, the fibres forming it are oriented at certain angles, θ.

In this case, the stress relation is written as given in Eqn (5).

$$\begin{bmatrix} \sigma_X \\ \sigma_Y \\ \tau_{XY} \end{bmatrix} = \begin{bmatrix} c^2 & s^2 & -2cs \\ s^2 & c^2 & 2cs \\ cs & -cs & -s^2 \end{bmatrix} \begin{bmatrix} \sigma_1 \\ \sigma_2 \\ \tau_{12} \end{bmatrix} = [T]^{-1} \begin{bmatrix} \sigma_1 \\ \sigma_2 \\ \tau_{12} \end{bmatrix} \tag{5}$$

$$[T] = \begin{bmatrix} c^2 & s^2 & 2cs \\ s^2 & c^2 & -2cs \\ -cs & cs & c^2 - s^2 \end{bmatrix} \tag{6}$$

The matrix [T] given herein is referred to as the transformation matrix and represents $c = \cos\theta$ and $s = \sin\theta$. Thus, stress and strain equations can be written in x-y and 1-2 coordinate systems as:

$$\begin{bmatrix} \sigma_1 \\ \sigma_2 \\ \tau_{12} \end{bmatrix} = [T] \begin{bmatrix} \sigma_X \\ \sigma_Y \\ \tau_{XY} \end{bmatrix} \tag{7}$$

$$\begin{bmatrix} \varepsilon_1 \\ \varepsilon_1 \\ \gamma_{12}/2 \end{bmatrix} = [T] \begin{bmatrix} \varepsilon_X \\ \varepsilon_Y \\ \gamma_{XY}/2 \end{bmatrix} \tag{8}$$

1.2 Failure Theories for Composite Structures

1.2.1 Maximum Stress Theory

According to the maximum stress theory, if any of the principal axes of the composite layer reaches or exceeds the limit of compression, tensile, and shear stresses of these directions, material failure occurs. Accordingly, the following statements are used[15]. For tensile stresses $\sigma_1 \geq F_{1t}, \sigma_2 \geq F_{2t}$, for compression stresses $\sigma_1 \geq F_{1c}, \sigma_2 \geq F_{2c}$, and for shear stresses $|\tau_{12}| \geq F_6$. The maximum tensile strength in direction 1 is F_{1t}, the maximum tensile strength in direction 2 is F_{2t}, the maximum compression strengths in direction 1 and 2 are F_{1c} and F_{2c}, respectively and the maximum shear strength in both 1-2 directions are denoted by F_6.

1.2.2 Maximum Strain Theory

In maximum strain theory, if any of the principal axes of the composite layer reaches or exceeds the limit of unit elongations or shear angle limit under applied loads in these directions, failure occurs. According to above definition, the following statements can be written for tensile strains[15] $\varepsilon_1 \geq \varepsilon_{1t}, \varepsilon_2 \geq \varepsilon_{2t}$, for compression strains $\varepsilon_1 \geq \varepsilon_{1c}, \varepsilon_2 \geq \varepsilon_{2c}$, and for shear angle offset $|\gamma_{12}| \geq \gamma_6$.

Where the maximum tensile unit elongation in direction 1 is ε_{1t}, the maximum tensile unit elongation in direction 2 is ε_{2t}, the maximum compression unit elongation in direction 1 is ε_{1c}, the maximum compression elongation in direction 2 is ε_{2c} and the maximum shear angle in plane 1-2 is denoted by γ_6. Stresses and shear angles can also be written in terms of strain:

$$\varepsilon_1 = \frac{(\sigma_1 - \nu_{12}\sigma_1)}{E_1} \tag{9}$$

$$\varepsilon_2 = \frac{(\sigma_2 - \nu_{21}\sigma_1)}{E_2} \tag{10}$$

$$\gamma_{12} = \frac{\tau_{12}}{G_{12}} \tag{11}$$

E, G and ν in these expressions refer to the Modulus of elasticity, Shear modulus, and Poisson's ratio in the related directions and planes, respectively. To calculate the maximum values, following equations can be written:

$$\varepsilon_1 = \frac{(\sigma_1 - \nu_{12}\sigma_1)}{E_1}, \; \varepsilon_2 = \frac{(\sigma_2 - \nu_{21}\sigma_1)}{E_2}, \; \varepsilon_{1c} = \frac{F_{1c}}{E_1},$$

$$\varepsilon_{2c} = \frac{F_{2c}}{E_2}, \; \gamma_6 = \frac{F_6}{G_{12}} \tag{12}$$

1.2.3 Tsai-Hill Theory

Tsai-Hill theory is a theory adapted from the Von-Mises theory for anisotropic materials. Accordingly, considering for the plane stress, material failure occurs if the following condition occurs[15].

$$\left(\frac{\sigma_1}{F_1}\right)^2 - \frac{\sigma_1 \sigma_2}{F_1^2} + \left(\frac{\sigma_2}{F_2}\right)^2 + \left(\frac{\tau_{12}}{F_6^2}\right)^2 \geq 1 \tag{13}$$

In this theory, no distinction is made between tensile and compression strengths. According to this;

$$F_1 = \begin{Bmatrix} \sigma_{1t}, & (\sigma_1 > 0) \\ \sigma_{1c}, & (\sigma_1 < 0) \end{Bmatrix}, \; F_2 = \begin{Bmatrix} \sigma_{2t}, & (\sigma_2 > 0) \\ \sigma_{2c}, & (\sigma_2 < 0) \end{Bmatrix} \tag{14}$$

To write the values as given in Eqn. (14) in σ_x, the following expressions can be used:

$$\sigma_1 = \sigma_x \cos^2\theta, \; \sigma_2 = \sigma_x \sin^2\theta$$

$$and \; \tau_{12} = -\sigma_x \sin\theta\cos\theta \tag{15}$$

From here to obtain the tensile strength;

$$\frac{1}{\sigma_x^2} = \frac{\cos^4\theta}{F_{1t}^2} + \frac{\sin^4\theta}{F_{2t}^2} + \left(\frac{1}{F_6^2} - \frac{1}{F_{1t}^2}\right)\sin^2\theta\cos^2\theta \tag{16}$$

for compression strength Eqn. (16) can be written as:

$$\frac{1}{\sigma_x^2} = \frac{\cos^4\theta}{F_{1c}^2} + \frac{\sin^4\theta}{F_{2c}^2} + \left(\frac{1}{F_6^2} - \frac{1}{F_{1c}^2}\right)\sin^2\theta\cos^2\theta \tag{17}$$

1.2.4 Tsai-Wu Theory

The Tsai-Wu theory is a simplified version of the theory of failure developed for anisotropic materials by Gol'denblat and Kopnov[15-16].

$$f_i\sigma_i + f_{ij}\sigma_i\sigma_j \geq 1, \; (i,j) = 1,2,3,4,5,6$$

$$f_1\sigma_1 + .. + f_6\sigma_6 + f_{11}\sigma_1^2 + .. + f_{66}\sigma_6^2 +$$

$$2f_{12}\sigma_1\sigma_2 + 2f_{13}\sigma_1\sigma_3 + 2f_{23}\sigma_2\sigma_3 \geq 1 \tag{18}$$

According to this theory, if the above statement takes 1 or bigger values, it is predicted that the material will fail. In the case of plane tension, this expression;

$$f_1\sigma_1 + f_2\sigma_2 + f_{11}\sigma_1^2 + f_{22}\sigma_2^2 +$$

$$f_{66}\tau_{12}^2 + 2f_{12}\sigma_1\sigma_2 \geq 1 \tag{19}$$

$$f_1 = \left(\frac{1}{F_{1t}} - \frac{1}{F_{1c}}\right), \; f_2 = \left(\frac{1}{F_{2t}} - \frac{1}{F_{2c}}\right),$$

$$f_{11} = \left(\frac{1}{F_{1t}.F_{1c}}\right) \; f_{22} = \left(\frac{1}{F_{2t}.F_{2c}}\right),$$

$$f_{66} = \frac{1}{F_6^2}, \; f_{66} = -\frac{1}{2}\sqrt{\frac{1}{F_{1t}.F_{1c}}.\frac{1}{F_{2t}.F_{2c}}} \tag{20}$$

1.2.5 Hashin Theory

Hashin theory is one of the most preferred theories. In this theory, the failure condition for the fibre is similar to the condition in the maximum tension theory. Fig. 2 shows the direction of the fibre denoted by 1, the direction of the matrix denoted by 2 and the number 3 represents the direction towards the thickness of the laminate layer. According to Hashin theory[17];

(a) If the following condition is satisfied for $\sigma_{11} > 0$, tensile failure occurs in direction 1.

$$\left(\frac{\sigma_{11}}{X_T}\right)^2 + \frac{\sigma_{12}^2 \sigma_{13}^2}{S_{12}^2} \geq 1 \tag{21}$$
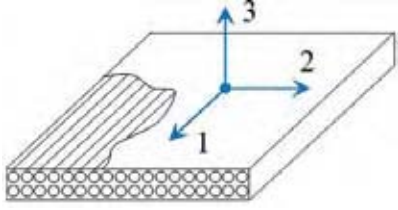
Figure 2. Coordinate axis for a 3D composite layer.

(b) If the following condition is satisfied for $\sigma_{11} < 0$, compression failure occurs in direction 1.

$$\left(\frac{\sigma_{11}}{X_C}\right)^2 \geq 1 \tag{22}$$

(c) If the following condition is satisfied for $\sigma_{22} + \sigma_{33} > 0$, tensile failure occurs in direction 2.

$$\frac{(\sigma_{23} + \sigma_{33})^2}{Y_T^2} + \frac{(\sigma_{23} - \sigma_{22}\sigma_{33})^2}{S_{23}^2} + \frac{\sigma_{12}^2 + \sigma_{13}^2}{S_{12}^2} \geq 1 \tag{23}$$

(d) If the following condition is satisfied for $\sigma_{22} + \sigma_{33} > 0$, compression failure occurs in direction 2.

$$\left[\left(\frac{Y_C}{2S_{23}}\right)^2 - 1\right]\left(\frac{\sigma_{22} + \sigma_{33}}{Y_C}\right) + \frac{(\sigma_{22} + \sigma_{33})^2}{4S_{23}^2} +$$

$$\frac{\sigma_{23}^2 - \sigma_{22}\sigma_{33}}{S_{23}^2} + \frac{\sigma_{12}^2\sigma_{13}^2}{S_{12}^2} \geq 1 \tag{24}$$

(e) If the following condition is satisfied for $\sigma_{33} > 0$, tensile failure occurs in direction 3.

$$\left(\frac{\sigma_{33}}{Z_T}\right)^2 \geq 1 \tag{25}$$

(f) If the following condition is satisfied for $\sigma_{33} < 0$, compression failure occurs in direction 3.

$$\left(\frac{\sigma_{33}}{Z_C}\right)^2 \geq 1 \tag{26}$$

According to the coordinate axis as shown in Fig. 3, the meanings of the symbols used in the above statements are as follows;

X_T : Maximum tensile strength in direction 1
Y_T : Maximum tensile strength in direction 2
Z_T : Maximum tensile strength in direction 3
X_c : Maximum compression strength in direction 1
Y_c : Maximum compression strength in direction 2
Z_c : Maximum compression strength in direction 3
S_{12} : Maximum shear strength in plane 1-2
S_{23} : Maximum shear strength in plane 2-3.

In the case of plane stress, the Hashin theory is expressed as:

(i) If the following condition is satisfied for $\sigma_{11} > 0$, tensile failure occurs in direction 1.

$$\left(\frac{\sigma_{11}}{X_T}\right)^2 + \left(\frac{\sigma_{12}}{S_{12}}\right)^2 \geq 1 \tag{27}$$

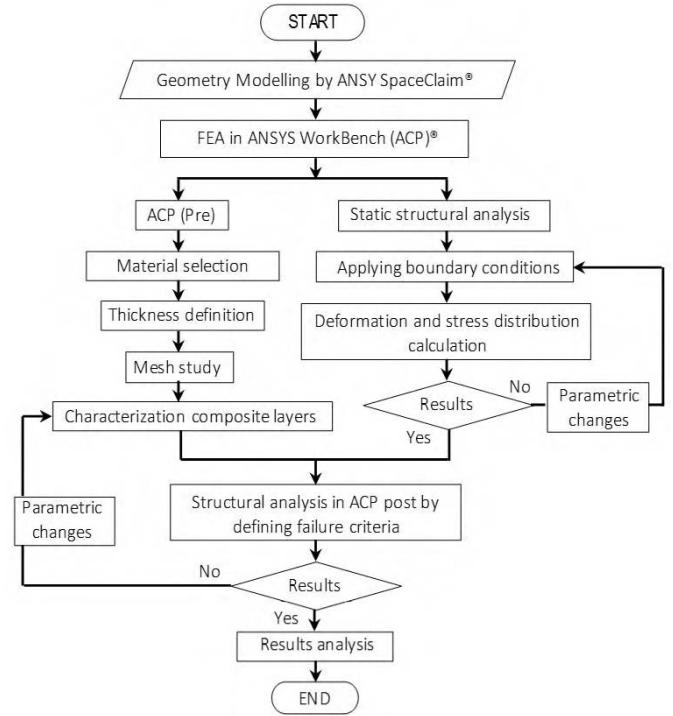(ii) If the following condition is satisfied for $\sigma_{11} < 0$, compression failure occurs in direction 1.

Figure 3. Schematic algorithm of pressure vessel analysis.

$$\left(\frac{\sigma_{11}}{X_C}\right)^2 \geq 1 \tag{28}$$

(iii) If the following condition is satisfied for $\sigma_{22} > 0$, tensile failure occurs in direction 2.

$$\left(\frac{\sigma_{22}}{Y_T}\right)^2 + \left(\frac{\sigma_{12}}{S_{12}}\right)^2 \geq 1 \tag{29}$$

(iv) If the following condition is satisfied for $\sigma_{22} < 0$, compression failure occurs in direction 2.

$$\left(\frac{\sigma_{22}}{2S_{23}}\right)^2 + \left[\left(\frac{Y_C}{2S_{23}}\right)^2 - 1\right]\left(\frac{\sigma_{22}}{Y_C}\right) + \left(\frac{\sigma_{12}}{S_{12}}\right)^2 \geq 1 \tag{30}$$

2. MATERIALS AND METHOD

ANSYS Workbench software was used to carry out the structural analysis of a composite winding pressure tank with finite element method. In this software, ANSYS Composite Pre-post (ACP)® module was used for more detailed modelling and analysis of composite structures. To create the analysis model, the solid model of the tank was made in ANSYS SpaceClaimCAD module. Then, both the liner and the composite part were modelled in preprocessing step. Figure 3 shows the flowchart of these steps. In this diagram, material properties of the composite structure, number and placement of layers and fibre angles are entered in ACP (Pre)® section and prepared for analysis. In modelling step, tank's liner is modelled (Mechanical Model). These two step are then combined for the static structural analysis to ensure that both the metal and composite parts of the tank are connected to each other. In "static structural analysis" section, analysis type, loadings and boundary conditions were entered and analyses were performed.

The ACP (Post) module is the section where the composite structure is analysed in detail in accordance with the failure theories. When forming the Section ACP (Pre), the properties of the Carbon-Fiber (TORAYCA T800H) are selected for the composite material and entered[18].

According to the information given by the manufacturer, the material is composed of 60 per cent fibre and 40 per cent Epoxy (volume fraction). The properties of the material formed for each layer are assigned. Then, layers were formed and a large number of linear analyses (~70) were performed to determine the number of layers. In order to find the ideal fibre angle for these layers[19], analyses were carried out by adjusting the fibre winding angles in the software to change parametrically. These analyses are repeated by increasing 1 degree in the range of 10 to 80 degrees. The results show the stresses on the liner and composite structure for each fibre angle in Fig. 4. Total composite thickness (18-layer x 0.8 mm) was obtained as 1.44 mm
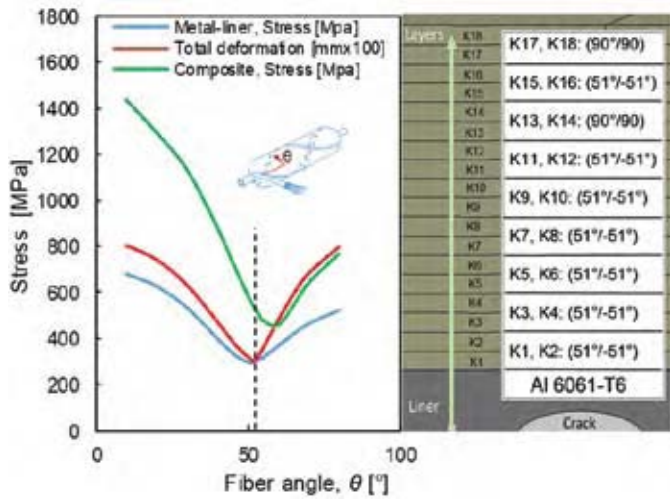

Figure 4. Ideal fiber angle (P=220 bar) and layer arrangement for composite wounded tank.

Carbon-fibre (TORAYCA T800H) / Epoxy composite and reinforcing fibre properties of the materials used in the analyses are as shown in Table 1 with respect to the fibre directions.

Table 1. T800H/Epoxy composite material properties[18]

Composite		Fibre	
Elasticity modulus E_z [GPa]	168	Elasticity mod. E_z [GPa]	294
Elasticity mod. E_x, E_y [GPa]	9.18	Tensile stren. [MPa]	5490
Shear mod. G_{xy}, G_{xz} [GPa]	5.55	Break elongation [%]	1.90
Shear mod. G_{yz} [GPa]	2.86	Density, ρ [kgm⁻³]	1800
Tensile strength [MPa]	2920	Filament dia. [μm]	5.00
Compression stren. [MPa]	1550		
Shear stren. [MPa]	164		
Poisson ratio v_{xy}, v_{xz}	0.33		
Poisson ratio v_{yz}	0.45		
Density, ρ [kgm⁻³]	1500		

Non-linear solution was used for Autofrettage and burst analysis. In order to carry out this analysis, the double-acting (line) isotropic hardening properties is activated in software for aluminum[20]. The material is elastic along the first and when the loading is lifted, the material can be returned to its original state. However, as the amount of loading is increased, there is a direct transition to the second line, which leads to strain hardening along the material[12]. The average modulus of elasticity in the elastic region can be calculated as 60 [GPa] and the average in the plastic region is 0.27 [GPa]. Passing from line 1 to line 2 corresponds to 276 MPa, which is actually the yield limit of the material. The mesh models, loading patterns and boundary conditions of the composite structure used in the finite element analyses are shown in the section given in Fig. 5. Six different types of elements namely, Tet10, Hex20, Wed15, Pyr13, Hex8 and Wed6, are used in the analysis. Type of contact is bonded and ANSYS Direct Solver is used in these analyses.
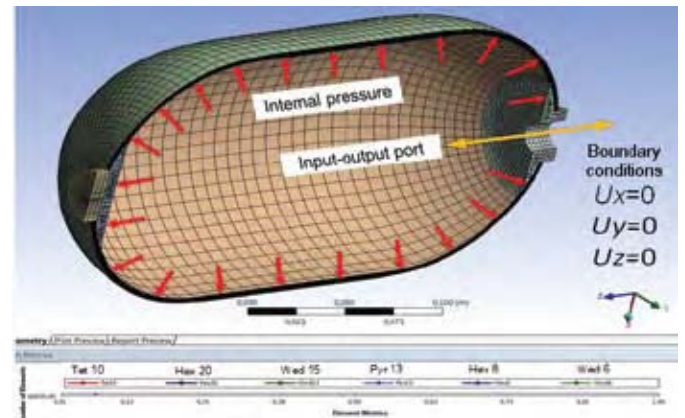

Figure 5. Finite element mesh model and boundary conditions of the liner.

According to the results, if the composite material is taken into consideration, the ideal fibre angle should be 59° (See Fig. 4). But the main consideration is the liner which is designed from Al6061-T6 material. The main part providing sealing is a liner and its strength is very low compared to the composite structure. For this reason, the lowest stress that may occur on the liner is taken into consideration and it is decided that the ideal fibre angle for helical winding is 51°. After determining the fibre angles of the layers, non-linear-analyses are performed to obtain more realistic results. As a result of a series of analyses, the layer array and fibre angles as shown in Fig. 4 are obtained to resist the possible slightest and desired pressure conditions for the tank.

The composite structure was formed by wrapping a total of 18 layers opposite to each other and at right angles. K 13-14 and K 15-16 are layers that are wrapped at right angles. In order to make structural design of a composite tank with composite winding, various requirements must be known. These requirements should be determined according to the purpose of the tank. The requirements as given in Table 2 are based on the ECSS standards[21] and the Xenon tank criterion[22] used on ETS VIII satellite, previously launched into space.

During the lifetime of the satellite which uses a propulsion system, a suitable tank volume of 9 kg Xenon, calculated

Table 2. Tank design criterion

Parameters	Requirements
Max.Exp.Op.Pres.(MOP)	170 bar-(Test: 50 repeat)
Test press. (MOP x 1.25)	212.5 bar(min.)-(5repeat)
Burst press. (MOP x 1.50)	255 bar(min.)
Fuel weight	9 kg Xenon gas
Tank weight	1.2 kg (max.)
Tank capacity	5 liter (min.)
Naturel frequency	>100 Hz
Failure type	Leakage before burst
Operating temperature	5°C-55°C

by considering the possible manoeuvres in orbit, must be determined. In order to determine the tank volume, it is necessary to know the isothermal lines of Xenon[23] which will be placed into the tank. Isothermal curves obtained at various temperatures for 9 kg Xenon tank show that a volume of approximately 5.3 liters is required at a pressure of 170 bar for a maximum design temperature of 55 ºC. With this information, considering the other design criteria, the mechanical design of the tank has been initiated. Nomenclature of the tank is as given Fig. 6. Mechanical structure of the composite wounded tank consists of a 0.6 mm novel thick aluminum liner that provides sealing in the interior and a Carbon-Epoxy composite material wrapped on the outer surface which increases the pressure resistance of this liner.

In pressurised vessels, the origin of the burst is caused by surface or similar internal defects due to manufacturing or operating conditions. Because of the stress concentrations around the fault, the crack is formed during the periodic operating pressure, and then these cracks propagate and cause tearing. By using elliptical or circular modelling of these cracks in the approaches of the analysis of errors, more exact estimation solutions have been produced which are very close to actual results. This type of approach was preferred in this study since the semi-elliptic error on the surface of the pressurised vessel and the elliptical error assumption in the interior state bring the solution to an optimum condition. The crack type used in these analyses is only elliptical fracture due to the similarity of real crack geometry. In figures and equations, t means liner thickness, a means crack depth and c means crack length. According to the results of these analyses, it is examined whether a cracking in the tank would occur
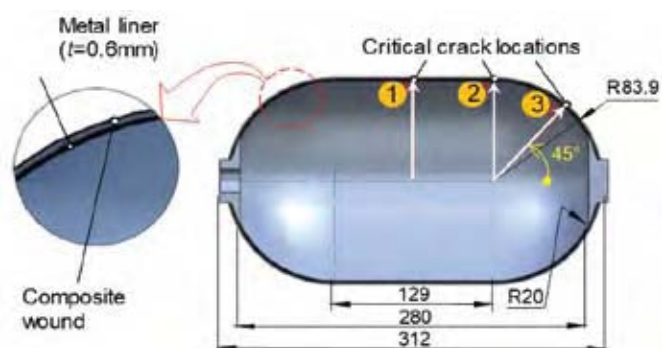
during the launch or during operations in space. In fact, the cracking or opening of the crack means the burst of the tank, which also means that it damages the structure inside the tank. Therefore, in such cases, it is desirable for the tank to leak slowly during the explosion so that the structures around the tank are not damaged or the collateral damage is minimised.

According to loading types, cracks are investigated in three different ways. These failure modes are opening, sliding and tearing respectively. The analyses were carried out for 3 different critical locations (1: cylinder, 2: CDT and 3: dome) of the tank as shown in Fig. 6 and for cracks at 0°, 45° and 90° angles in each location. The cylinder axis of the tank here represents 0° angle.

In this study, both the welding regions and the regions exposed to high stress are considered critical zones in terms of cracks. For cracks at angles of 0°, 45° and 90°, five different crack types were investigated, starting from a/c ratio of 1/5 and 2/5, 3/5, 4/5 and 5/5. For the liner having a thickness of 0.6 mm, which is the thinnest thickness in the literature, a value (depth of crack) of 0.5 mm was taken as the maximum and the analyses were carried out by changing in the above ratios. Figure 7 shows an exemplary numerical mesh model and angular (0°, 45° and 90°) orientation used in crack analysis. Owing to perform the analysis in the ANSYS Workbench V14.5, the element types used in the digital network can only be tetrahedron elements.

Another aspect is radial buckling; the liner may expose to the radial buckling due to the roving tension during winding. In this study, for winding process, the required roving tension is between 30 N to 40 N and a servo-controlled machine with fibre tension system that equipped with load cells is used. With 5 mm roving width and 40 N roving tension, approximately 0.2 MPa roving pressure is occurred on the liner surface during
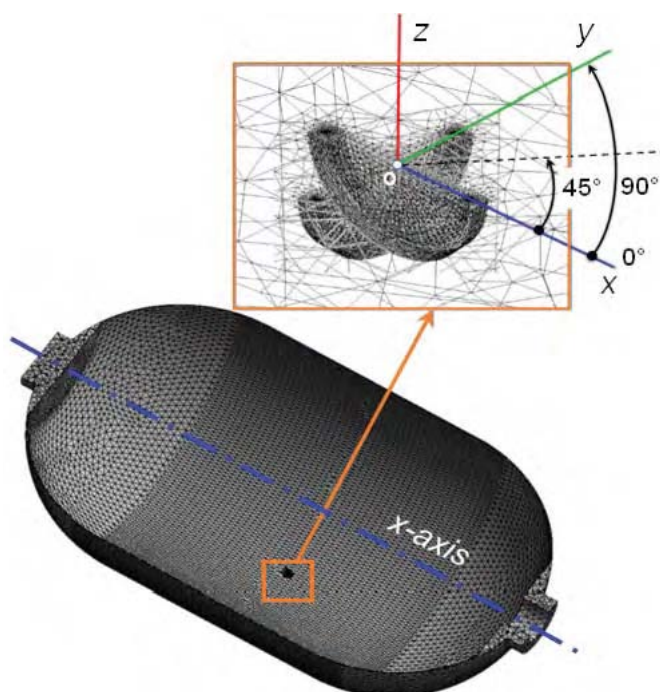

Figure 6. Filament wounded type-3 composite pressure vessel and its dimensions (mm).

Figure 7. FE crack mesh model and its 0°, 45° and 90° orientation angles.

winding. According to the Koiter's buckling theory, the critical pressure is calculated as follows[24];

$$P_{cr} = \frac{2Et^2}{R^2\sqrt{3}(1-\upsilon^2)} \qquad (31)$$

where, E is modulus of elasticity, R is tank radius, t is liner thickness and υ is Poisson ratio. The critical (collapsible) pressure is obtained as 4.37 MPa. Also considering the hoop yielding in compression will occur at yield pressure;

$$P_y = \frac{\sigma_y t}{R} \qquad (32)$$

where, σ_y is yield strength of liner. And the yield pressure is calculated P_y=1.97 MPa. Since the pressure during winding is much lower than the critical buckling pressure (0.2 MPa<<P_{cr}=4.37 MPa), and hence, no buckling will occur under proposed loading conditions during winding.

Furthermore, modal analyses and random vibration effects were investigated. No significant impact was observed in terms of launching and flight, assembly and space conditions. Hence, vibrational aspects were not given in this paper. For the health of other satellite equipment, the temperature in the satellite is kept between 0 °C and 50 °C with the thermal control system. Furthermore, since the Xenon fuel becomes unstable at about 16.6 °C, the tank temperature is maintained between about 20 °C and 50 °C. To keep the working temperature of the tank between 20-50 °C, electrical heaters connected to the thermal control system are used. Therefore, thermal effects were not investigated in this study.

3. AUTOFRETTAGE ANALYSIS

The composite wounded pressure tanks are subjected to a further processing after the filament winding process is completed. This process pressurises the composite tank so that the yield strength of the liner is exceeded and the inner surface of the liner is subjected to plastic deformation. The maximum tensile strength of the metal is not exceeded during this process. This production process is called Autofrettage. The pressure applied to the tank during the Autofrettage process is a value between the test pressure and the burst pressure. The Autofrettage process is a process which increases the fatigue life of the pressure tanks[25] prevents the crack development and increases the compressive strength[28]. By this method, low-cost materials are used for high-strength applications[28]. The Autofrettage process can be expressed in two stages. In the first stage, high pressure is applied and due to this high pressure, plastic deformation is present in the interior of the part and it shows an elastic behaviour when going outward. After the pressure is reset again, in the second step, a compressive force is formed on the inner surface of the part while the outer portion is attempting to return elastically. By means of this pre-stress, the compressive strength of the part is increased.

In the analyses, various pressurisation stages were used to see the effect of Autofrettage. These stages were first as shown in Fig. 8, starting with the maximum operating pressure (MOP) of 170 bar, and then reducing the pressure to 0 bar, which was then repeated to show that there was no change in the liner at
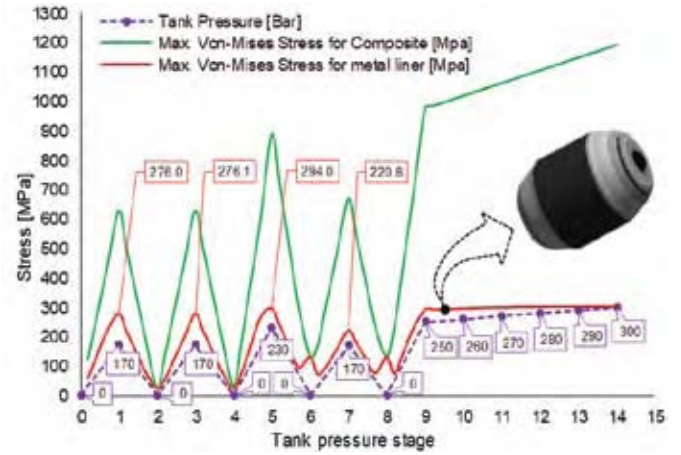

Figure 8. Autofrettage and burst stages with pressurisation.

this pressure. In step 6, when the pressure in the tank is lowered to 0 bar. In step 5, 230 bar was used as an Autofrettage pressure. This pressure is a pressure between 1.25xMOP test pressure and 1.5xMOP bursts pressure. In this analysis the Autofrettage pressure is approximately 1.35xMOP. The maximum stress on the liner when Autofrettage is applied is approximately 294 MPa. This value is higher than the yield limit of 276 MPa[29] and lower than 310 MPa,[29] the maximum tensile strength of the metal. This shows that the selected Autofrettage pressure is appropriate for this configuration.

The pre-tension formed in the liner can easily be observed. In step 7, the pressure inside the tank was increased to 170 bar, which was again the operating pressure, and at this stage the stress formed on the liner was approximately 221 MPa. This value was about 276 MPa before Autofrettage. This shows that the compressive strength of the tank increases as a result of the Autofrettage process. Von Mises stress and maximum shear stress results seen on the both liner before and after the Autofretage depending on the pressure like in the previous studies[6, 29-30]. The results show that the maximum shear stress on the liner before Autofrettage is about 158 MPa. There is also a shear stress of approximately 159 MPa during the Autofrettage step, i.e. 230 bar pressurisation stage. These values are below 207 MPa shear stress[25] given for Al 6061-T6. Therefore, there will be no failure due to shear stress in the Autofrettage stage in the liner. Since this designed fuel tank will be used after Autofrettage, as shown in step 7, the maximum shear stress in the operating pressure of 170 bar (MOP) applied after Autofrettage is about 117 MPa. Again, as expected, a significant reduction in shear stress was also observed due to Autofrettage. When deformation results are examined, maximum 0.5 mm deformation occurs during Autofrettage, while in step 7, maximum deformation is 0.38 mm under pressure of 170 bar. The maximum deformation occurs on the circumference of the tank (See Fig. 9).

The pressure in the tank is gradually increased to 300 bar to determine the bursting pressure. The bursting state of the tank cannot be understood from Fig. 8. Therefore, it should be checked whether the composite material on the liner is damaged. If there is damage to the composite material, it can be interpreted that there will be bursting. With the ANSYS
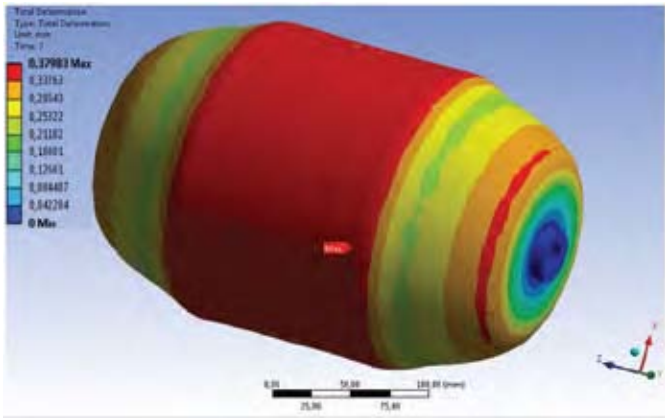
Figure 9. Total deformation in liner (Stage 7: 170 bar).

software, composite failure criteria i.e. theories which are described in previous sections are examined. The ACP (post) module was used to examine these failure criteria in ANSYS software. With this module, it can easily be seen in which stage of the composite material, which layer and according to which criteria the failure occurs. Figures 10 and 11 show the damage cases that have occurred in the most important stages and in the most critical layers.

In these figures, the meaning of abbreviations shown on each element summarised as follow:

s_1, s_2 : Maximum stress
e_1, e_2, e_3 : Maximum strain
th : Tsai-Hill
tw : Tsai-Wu
hf, *hm*, *hd* : Hashin, (here, *hf*: fibre failure, *hm*: matrix failure and *hd*: delamination failure) expresses the criteria. The abbreviations shown on each element represent the criteria with the highest value among these 5 different criteria.
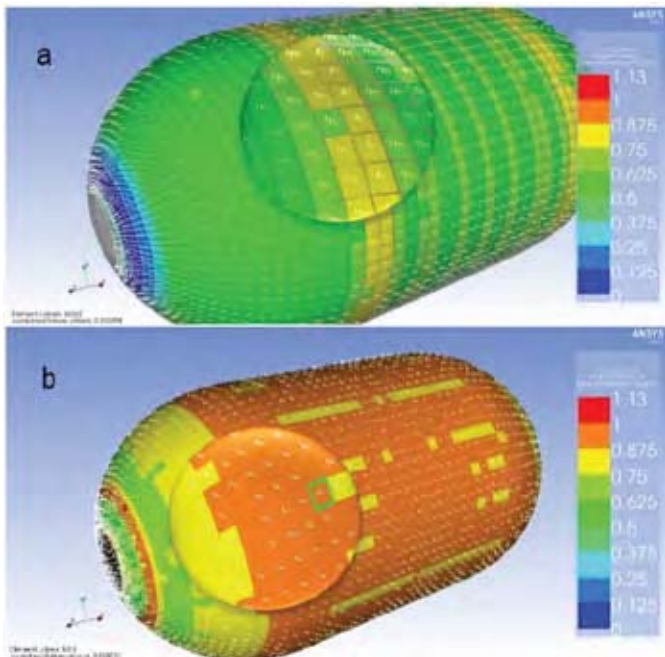

Figure 10. Composite damage condition of tank at pressure of (a) 230 (lay. 16) and (b) 280 bar (lay. 1).
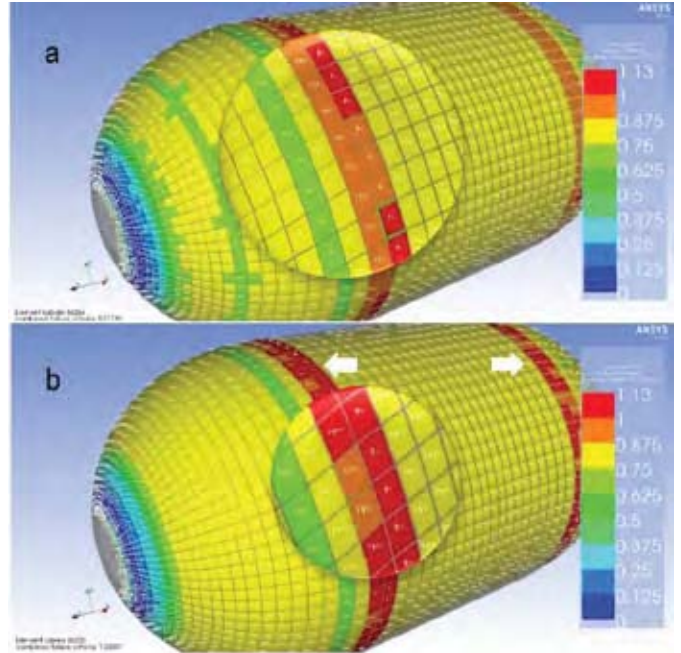

Figure 11. Composite damage of the tank at (a) 280 bar (Layer 16) and (b) 290 bar pressure (layer 16).

According to these criteria, it is understood that damage will occur in areas with damage status 1 and above, which is indicated by red color code. According to the analysis of maximum stress and maximum strain theories (denoted by *s*1, *s*2 and *e*1, *e*2, *e*3, respectively), no critical regions were found. The calculations according to these two theories were more secure than the theories representing *th*, *tw*, *hf*, *hm,* and *hd* regions. In Fig. 11(a), the composite material does not receive any damage at 230 bar pressure during the Autofrettage process.

The layer 16 shown in Fig. 11 here shows the most critical layer in all composite layers. In the colour code map, the green regions represent the areas that formed according to the *hm* criterion, while in the yellow regions which approaching a little more critical value represent the areas that formed according to the *th* criterion. In order to determine the burst pressure, it is seen that when all the pressurisation stages are followed, the composite material starts to take damage at 280 bar pressure. Figure 11 shows the damage conditions of the most critical 2 layer under (a) 280 and (b) 290 bar pressure. Although there is no damage in layer 1 according to Fig. 10(b), it is shown that the circumference region reaches the limit stress values according to *tw*. In Fig. 11, the red regions increasing with the transformation of orange regions and therefore, the CDT regions are more clearly visible with increasing pressure.

4. FRACTURE ANALYSIS

The crack analysis was carried out to ensure that the tank pressure was 220 bar (~1.3xMOP) in order to remain on the safe side for real experiments. The pressure of 220 bar was chosen slightly above the test pressure of 212.5 bar. In order to evaluate the results of the analysis, *J*-integral and *K* (stress intensity factor) values of cracks in various sizes were

compared. The *J*-integral is known as the elastic-plastic damage parameter found by James R. Rice in 1968.

The *J*-integral method is used to determine the amount of change in potential energy resulting from the progress of a crack. So, it is an indication of whether there will be a propagation in the crack or not. For the calculation of *J*-integral as shown in Fig. 12, an arbitrary line is formed around a crack, and line integral is taken along this line.[5-7] The expression of independent line integral is as shown in Eqn. (33)[5-8].

$$J = \int_{\Gamma} \left(wdy - T_i \frac{\partial u_i}{\partial x} ds \right) \tag{33}$$

In the above equation, *w* represents the stress energy density, T_i represents the stress vector components, u_i represents the displacement vector components and *ds* represents the length piece taken along with line Γ.

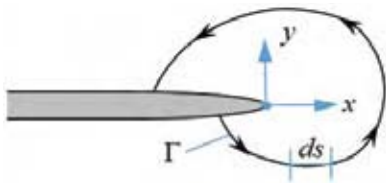In order to find the stress energy density (*w*) as given in

Figure 12. An arbitrary line created at the end of a crack.

Eqn. (33), the following equation is used. The expression σ_{ij} as given in the Eqn. (34) refers to the tensile tensor and ε_{ij} is the strain tensor. The *J*-integral values obtained by the finite element analysis are as shown in Fig. 13.

$$w = \int_0^{\varepsilon_{ij}} \sigma_{ij} d\varepsilon_{ij} \tag{34}$$

When these graphs are examined, the maximum energy intensity values generally occur at 0° crack angle independently from the region, while the lowest values are at 90° crack angles in the same regions (See Fig. 13). The *J*-integral value decreases as the ellipse geometry approaches to the circle geometry, i.e. the *a/c* ratio increases. In the case of full circle (*a/c*=5/5) and around the 1 radian angle (90°), lower energy discharge value than all *a/c* values are obtained[31]. On the other hand, the lowest *J*-integral values were obtained in the 1st location (cylinder region) and 90° crack orientation angle. The most critical orientation angle is zero for all positions in terms of fracture propagation probability.

However, regardless of the orientations, the locations with the highest probability of crack propagation occur in the 2nd locations (CDT regions). Namely, in the *J*-integral graphs given below, it is determined that the most critical cracking region is 2 and the most critical cracking angle value is 0°.

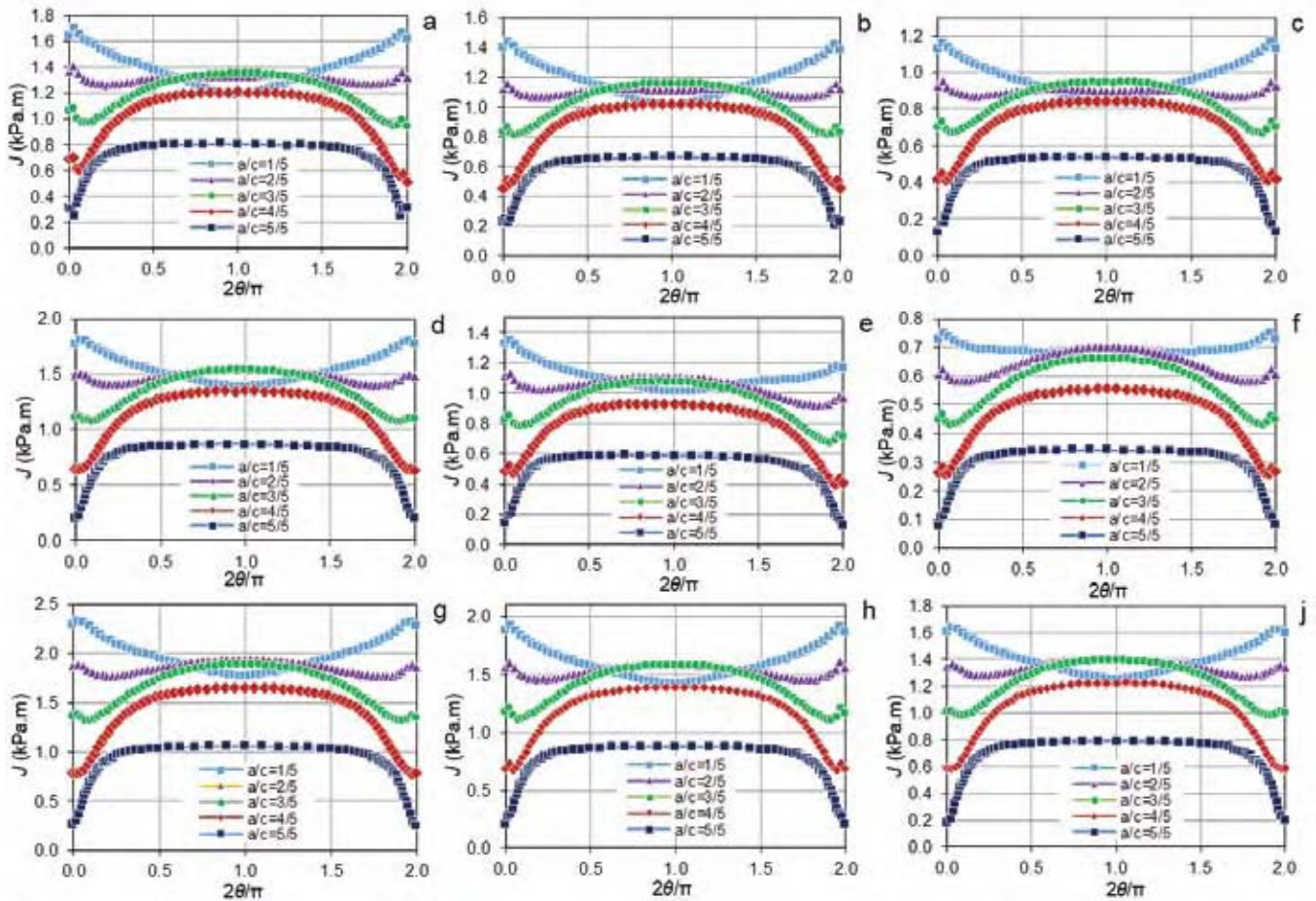The reason why the CDT region is more suitable for crack

Figure 13. *J*-integral graphs for cracks at (a) 0°, (b) 45° and (c) 90° orientation angles at critical location 1 (cylinder), (d) 0°, (e) 45° and (f) 90° orientation angles at critical location 2 (CDT) and (g) 0°, (h) 45° and (j) 90° orientation angles at critical location 3 (dome).

development is primarily due to the high stresses occurring under the high-pressure load during Autofrettage and the resulting large deformations (See in Section 3, Figs. 10 and 11).

$$J_c = \frac{(1-v^2)}{E} K_{IC}^2 \qquad (35)$$

In order to determine whether there is any progress in this crack, the critical value of *J*-integral should be calculated. The J_c value of *J*-integral is derived as (35) for plane strain condition[7, 31].

For Aluminum alloy (6061-T6), the *v*, *E* and K_{IC} values[8] are calculated as J_c = 10.86 [kPa.m] when substituted in Eqn. (33). This value is as shown in Fig. 14 as a red line showing the most critical crack state when redraw the Fig. 13(d). Since *J*-integral values obtained as a result of analysis according to Fig. 13(d) (location 2/crack angle 0°) are much smaller than J_c value, it is foreseen that the crack will not propagate and there will be no burst even in the most critical crack condition for given loadings. In addition, the crack length, i.e. the *c* value was also examined to investigate the effect on crack propagation. For this purpose, the most critical crack location 2 and the 0° crack angle condition were discussed and scenarios were created.
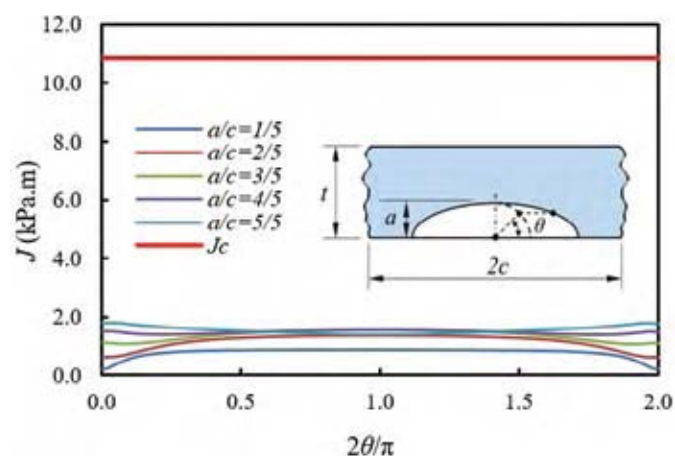

Figure 14. Comparison of *J*-integrals formed in critical crack region with J_c.

As can be seen in Fig. 15, the semi elliptical length increases the *J*-integral values under constant depth of crack value. The *c* value can be changed in the range of 1 mm to 5 mm, provided that *a* = 0.5 mm value is kept constant for these internal surface cracks. Under these conditions the critical value of *J*-integral does not exceed 10.86 [kPa.m] value and it is revealed that, even cracks up to *c* = 5 mm, the cracks do not propagate.

The liner part of the fuel tank consists of two dome and a cylinder body. These parts were produced by methods such as deep drawing and machining, and then they were combined with electron beam welding technique and made ready for testing. The liner was checked by non-destructive testing with X-Ray after welding. As a result of the inspection, no nonconformity was detected within the scope of welding process.

Pressurisation tests were performed at room conditions in a vacuum measuring vessel by pressing helium gas at a maximum operating pressure (MOP) of 170 bar. The sealing
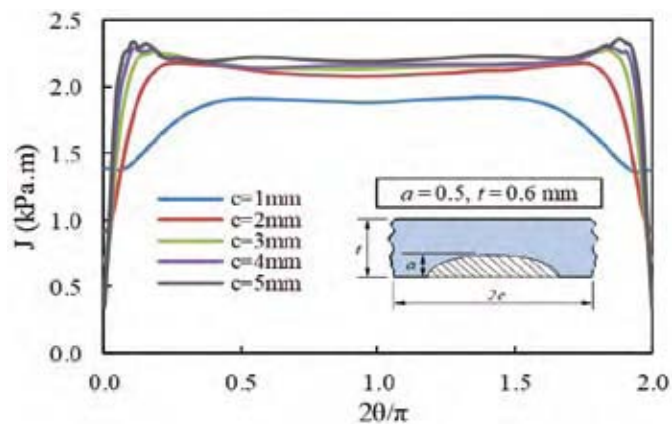

Figure 15. *J*-integral for scenarios created for the most critical condition (*a* = 0.5 and *c* = 1, … 5 mm).

measurement was continued for 1 h and the measured value obtained in the last 5 min was found to be below 10^{-6} sec per second. No buckling was found after the pressurisation tests. Bursting test is a test performed at the final stage of fuel tank qualification tests. In accordance with the previously obtained requirements, the tank bursting pressure was applied at room temperature at least twice the operating pressure. The pressurisation test device and the exploded stage of the Type-3 tank produced according to the measurements obtained from the design calculations and analyses are shown in Fig. 16(a) and Fig. 16(b), respectively.

As a result of the fuel tank bursting test, the test model burst at approximately 396 bar. It has been found that the design requirement mentioned in the previous sections is more than met. After the surface examination, it was observed that the onset of burst developed in the direction of CDT (See Fig. 16(b)). It was observed that the experimental results gave close values to the analysis results. Due to the privacy of this study, more detailed information about the test methods, test results and obtained data could not be given.
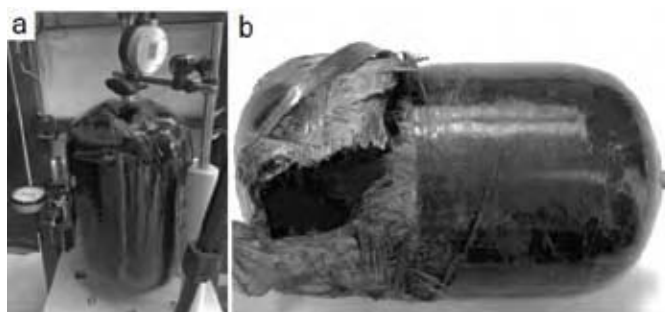

Figure 16. Tank bursting test (a) pressurisation test setup and (b) burst composite tank.

5. DISCUSSION

Effect of Location: Studies in the literature show that the most critical locations in the pressurised liner-composite winding vessels are the CDT regions (location 2). The most critical area for stress-strain after CDT regions is the cylinder region (Location 1). The tertiary critical region is determined as a dome region (location 3)[12-13].

Effect of Orientation Angle: Fakoor[9], *et al*. reported that

zero degree semi-elliptical internal and external cracks in the 1st location (cylinder region) were the most critical orientation angle for crack formation and development as a result of the finite element analysis. In this study, the most critical orientation angles occur at zero degrees for all locations.

Effect of Crack size: In the study of Hu & Chandrashekhara[6], the *J*-integral values are calculated for the Type 3 pressure vessel with Carbon-Epoxy composite wrapped on a 2.54 mm (1 in.) thick Al7075-T6 aluminum alloy liner.

Calculations are made according to semi-elliptical crack under constant load of 1.5 x MOP and the results are as shown in Fig. 17 as a small graph. When the *J*-integral values obtained from this study are compared under similar conditions, i.e. equal *a/c* ratio and constant thickness, it is seen that the *J*-integral values increase as the *a/c* ratio decreases and decreases in the opposite case. These comparisons show that the finite element model established in this work and numerical computations carried out give close results with the literature.

Considering the burst pressure, the thickness of the liner examined here is much smaller than the liner thicknesses examined in the literature, and in FEM calculations, the strength values are slightly lower than the Al 6061 T6 standard values due to welded joints, resulting in low bursting pressure. However, when the strength and wall thickness parameters are compared, approximate results are obtained with the literature[4,12,24-25].
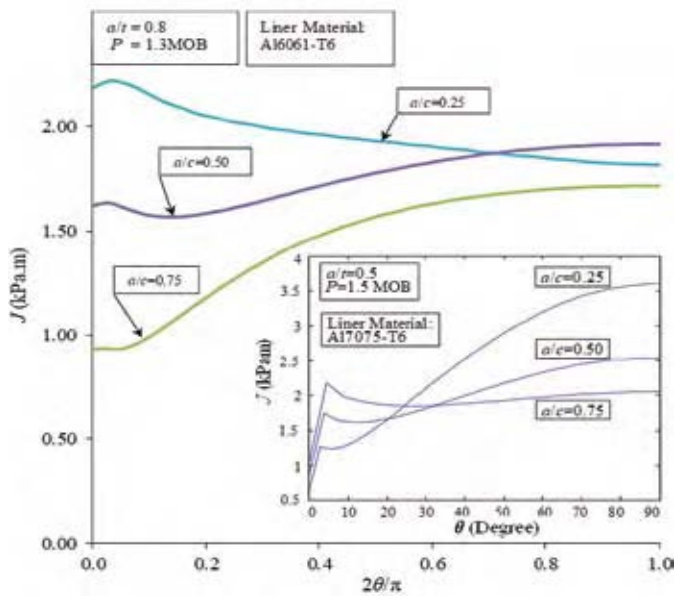

Figure 17. A comparison of *J*-integral values for different *a/c* ratios with Reference 6.

6. CONCLUSIONS

In this work, the design and analysis stages of a composite winding pressure tank have been investigated for use in a military satellite electric propulsion system. The design requirements have been established in accordance with ESA standards, considering the need for a 9 kg Xenon fuel need, operating conditions in space, launching loads and other technical requirements. Using ANSYS Workbech® and ACP® software, a finite element analysis model which composed of Aluminum liner (Al6061-T6) and Carbon-fibre/

Epoxy composite layers formed by over wrapping is created. According to this model, crack analyses are performed by using finite element method. As a result of the stress-strain analysis, the optimum fibre helical winding angle is determined as 51°. Fracture analyses show that the most critical location is cylinder dome transition (CDT) region and the most critical crack orientation angle is 0°. For constant crack depth, *J*-integral value increases with increasing crack length. However, when the ratio of depth over length of the crack is increases *J*-integral value decreases. Finally, it is predicted that even in the most critical case, the crack will not propagate and there will be no burst in proposed pressure vessel for the given loading conditions.

REFERENCES

1. Liu, P.F.; Chu, J.K.; Hou, S.J.; Xu, P. & Zheng, J.Y. Numerical simulation and optimal design for composite high-pressure hydrogen storage vessel: A review. *Ren. Sust. Ener. Rev.*, 2012, **16**, 1817-1827.
   doi: 10.1016/j.rser.2012.01.006

2. Madhavi, M.; Rao, K.V.J. & Rao, K.N. Design and analysis of filament wound composite pressure vessel with integrated-end domes. *Def. Sci. J.*, 2009, **59**(1), 73-81.

3. Kaikai, S.; Lixun, C.; Long C. & Chen, B.; A theoretical model of semi-elliptic surface crack growth. *Chin., J. Aerona.*, 2014, **27**(3), 730-734.
   doi: 10.1016/j.cja.2014.04.012

4. Xu, P.; Zheng, J.Y. & Liu, P.F. Finite element analysis of burst pressure of composite hydrogen storage vessels. *Mater. Desig.* 2009, **30**, 2295-2301.
   doi: 10.1016/j.matdes.2009.03.006

5. Wang, J.; Jiang, W.; Li, Y.; Wang, Q. & Xu, Q. Numerical assessment of cyclic *J*-integral Δ*J* for predicting fatigue crack growth rate. *Eng. Frac. Mech.*, 2019, **205**, 455-469.
   doi:10.1016/j.engfracmech.2018.11.031

6. Hu, J. & Chandrashekhara, K. Fracture analysis of hydrogen storage composite cylinders with liner crack accounting for autofrettage effect. *Int. J. Hydrogen Energ.*, 2009, **34**, 3425-335.
   doi:10.1016/j.ijhydene.2009.01.094

7. Zhu, X. J-integral resistance curve testing and evaluation. *J. Zhejiang. Univ-Sci A (Appl. Phys. & Eng.)*, 2009, **10**(11), 1541-1560.
   doi:10.1631/jzus.A0930004

8. Murtaza, U.T. & Hyder, M.J. The effect of thermal stress on the elliptical surface cracks in PWR reactor pressure vessel. *Theor. Appl. Fract. Mech.*, 2015, **75**, 124-136.
   doi: 10.1016/j.tafmec.2014.12.001

9. Fakoor, M.; Ghoreishi, S.M.N. & Khansari, N.M. Investigation of composite coating effectiveness on stress intensity factors of cracked composite pressure vessels. *J. Mech. Sci. Technol.*, 2016, **30**(7), 3119-3126.
   doi:10.1007/s12206-016-0621-8

10. Park, J.S.; Hong, C.S.; Kim, C.G. & Kim, C.U. Analysis of filament wound composite structures considering the change of winding angles through the thickness direction.

Compos. Struct., 2002, **55**, 63-71.

11. Crabonari, R.C.; Munoz-Rojas, P.A.; Andrade, E.Q.; Paulino, G.H.; Nishimoto, K. & Silva, E.C.N. Design of pressure vessels using shape optimization: An integrated approach. *Int. J. Pres. Ves. Pip.*, 2011, **88**, 198-212.
doi:10.1016/j.ijpvp.2011.05.005

12. Zu, L.; Xu, H.; Wang, H.; Zhang, B. & Zi, B. Design and analysis of filament-wound composite pressure vessels based on non-geodesic winding. *Compos. Str.*, 2019, **207**, 41-52.
doi:10.1016/j.compstruct.2018.09.007

13. Almeida Jr, J.H.S.; Faria, H.; Marques, A.T. & Amico, S.C. Load sharing ability of the liner in type III composite pressure vessels under internal pressure. *J. Reinf. Plast. Comp.* 2014, **33**(24), 2274-2286.
doi:10.1177/0731684414560221

14. Reddy, J.N. Mechanics of laminated composite plates and shells: Theory and analysis. Ed. 2nd. CRC Press LLC, Boca Raton, Florida, U.S.A, 2004.

15. Daniel, I.M. & Ishai, O. Engineering mechanics of composite materials. Oxford University Press, New York, U.S.A., 1994.

16. Paknahad, A.; Fathi, A.; Goudarzi & Nourani, A. M. Optimum head design of filament wound composite pressure vessels using a hybrid model of FE analysis and inertia weight PSO algorithm. *Int. J. Mater. Form.* 2014.
doi: 10.1007/s12289-014-1199-2

17. Hashin, Z. Failure criteria for unidirectional fibre composites. *J. Appl. Mech-T. ASME*, 1980, **47**, 329-334.

18. Toray Carbon Fibers America Inc., http://www.toraycfa.com/pdfs/T800HDataSheet.pdf [Accessed on 16 November, 2016].

19. Onder, A.; Sayman, O.; Dogan, T. & Tarakcioglu, N. Burst failure load of composite pressure vessels. *Compos. Struct.*, 2009, **89**, 159-166.
doi: 10.1016/j.compstruct.2008.06.021

20. ANSYS Workbench Software Material Library, ANSYSY Inc. 2014.

21. European Cooperation for Space Standardization, ECSS-E-10-03A, Space Engineering: Testing, 15 February 2002.

22. Tam, W. H.; Jackson, A. C.; Nishida, E.; Kasai, Y. Design and manufacture of The ETS VIII Xenon Tank. AIAA2000-3677.

23. The National Institute of Standards and Technology, Isothermal Properties for Xenon, http://webbook.nist.gov/chemistry/fluid/ [Accessed on 12 April, 2017].

24. Zhu, Y.; Zhang, Y.; Zhao, X.; Zhang, J. & Xu, X. Elastic-plastic buckling of externally pressurized hemispherical heads. *Ships Offshore Str.*, 2019, **14**(8), 829-838.
doi: 10.1080/17445302.2018.1564541

25. Han, M.G. & Chang, S.H. Failure analysis of a Type III hydrogen pressure vessel under impact loading induced by free fall. *Compos. Str.*, 2015, **127**, 288-297.
doi: 10.1016/j.compstruct.2015.03.027

26. Cho, S.M.; Kim, K.S.; Lee, K.M.; Lee, S.; Lee, Y.J. & Lyu, S.K. A study on cycling life and failure mode of Type3 cylinder treated with autofrettage pressure. *Int. J. Precis. Eng. Man.*, 2016, **17**(1), 1685-1691.
doi: 10.1007/s12541-016-0195-5

27. Maximator Test, LLC, White Paper-Autofrettage, http://www.maximator-test.com/about/White-Paper-Autofrettage.pdf, [Accessed on 8 May, 2014].

28. ASM Material Data Sheet, Aluminum 6061-T6, http://asm.matweb.com/search/SpecificMaterial.asp?bassnum=MA6061t6 [Accessed on 17 November, 2016]

29. Multhoff, J.B. Effective structural design procedure for composite hydrogen tanks. *In* 18th World Hydrogen Energy Conference, Essen, Germany, 2010.

30. Liao, B.B.; Wang, D.L.; Jia, L.Y.; Zheng, J.Y. & Gu, C.H. Continuum damage modeling and progressive failure analysis of a Type III composite vessel by considering the effect of autofrettaga. *J. Zhejiang. Univ-Sci A (Appl. Phys. & Eng.)*, 2019, **20**(1), 36-49.
doi: 10.1631/jzus.A1800152

31. English, S.A.; Arakere, N.K. & Allen, P.A. J–Q characterized stress fields of surface-cracked metallic liners – II. Composite overwrapped pressure vessels. *Eng. Frac. Mech.*, 2011, **78**, 2097-2114.
doi:10.1016/j.engfracmech.2011.02.023

ACKNOWLEDGEMENT

CONTRIBUTORS

Mr Muzaffer Çetin completed his BS (Mechanical Engg.) from Middle East Technical University, in 2006 and MSc (Mechanical Engg.) from Hacettepe University in Ankara, Turkey, in 2014. He is currently a Chief Researcher at Department of Mechanical Design in Space Technologies Research Institute, The Scientific and Technical Research Council of Turkey. His research interests include the fields of fracture and composite structure analysis and finite element modelling.
In current study, he has extended the theoretical equations and carried out the winding angle, Autofrettage and fracture analyses.

Dr Kemal Yaman is a chief Researcher in The Scientific and Technological Research Council of Turkey, Defense Industries Research and Development Institute (TUBITAK SAGE) in Mechanical Systems Group. He completed his BS, MSc and PhD in Mechanical Engineering from Gazi University in Ankara in 1998, 2002, and 2007 respectively. His research interests include the fields of mechanics of materials, fatigue and fracture testing and analysis, composite materials and structural analysis, finite element modelling and analysis.
In current study, he contributed to processes of testing and manufacturing of fuel tank, literature survey on the related topics and reviewed the paper.